2022

R1234ze(E) as a Low-GWP Replacement of R410A in Fin-and-Tube Evaporators

Saad Saleem

Craig R. Bradshaw

Christian K. Bach

R1234ze(E) as a Low-GWP Replacement of R410A in Fin-and-Tube Evaporators

Saad SALEEM[(a)]*, Craig R. BRADSHAW[(b)], Christian K. BACH[(c)],

(a) Energy, Sustainability & Infrastructure (ES&I) segment, Guidehouse, Burlington, MA 01803, USA
(b) (c) Center for Integrated Building Systems, Oklahoma State University,
Stillwater, OK 74078, USA
(a) saad.saleem@okstate.edu, (b) craig.bradshaw@okstate.edu, (c) cbach@okstate.edu
(a) (+1)405-762-1293, b) (+1) 405-774-5246, (c) (+1) 405-744-5916

* Corresponding Author

ABSTRACT

Regulatory requirements throughout the world are compelling air conditioning (AC) and heat pump (HP) manufacturers to switch from halogenated refrigerants, like R410A, to more environmentally friendly alternatives with reduced global warming potential (GWP). This study explores the ramifications of using the ultra-low-GWP refrigerant R1234ze(E) in a fin-and-tube evaporator coil designed for R410A. A total of 36 tests were carried out using a high-fidelity experimental facility for both refrigerants to validate a segment-by-segment heat exchanger model. R410A had a mean absolute percent error (MAPE) of 0.9% between experimental and simulated capacity, whereas R1234ze had an MAPE of 1.4%. Simulations with R1234ze(E) where then carried out, investigating the effects of modified fin density and refrigerant circuitry. Increasing the fin density of the baseline evaporator from 15 to 20 fins per inch (FPI) led to an increase in capacity of 4.9%, and a reduction in refrigerant side pressure drop of 4.5%. When comparing the refrigerant circuitry optimization to the baseline, a maximum increase in capacity of 5.6% was observed, but at the cost of 7.5 times higher pressure drop. An alternate heat exchanger circuitry resulted in a 38% reduction in pressure drop and a 2.5% reduction in capacity. The results showed that the chosen two heat exchanger geometrical parameters had a significant impact on capacity and refrigerant side pressure drop for R1234ze(E), indicating room for improvement in coil performance with low-GWP refrigerants by further adjusting heat exchanger geometry.

1. INTRODUCTION AND MOTIVATION

R410A is one of the most commonly used refrigerants in residential and light commercial Heating, Ventilation, Air Conditioning & Refrigeration (HVAC&R) systems. It has a high Global Warming Potential (GWP) of 2,088. Several regulatory measures worldwide, such as the F-gas Regulations, the Kigali amendment to Montreal Protocol, and most recently, a rule proposed by the US Environmental Protection Agency (EPA) under the American Innovation and Manufacturing Act rule (AIM, 2021), have called for gradual phase out of hydrofluorocarbons (HFCs), such as R410A. Thus, R410A needs to be replaced by suitable lower GWP substitutes, and its phase out will require substantial redesign efforts for HVAC&R equipment.

Extensive research effort to find short term low-GWP alternatives to R410A (Sethi & Motta, 2016, Devecioğlu, 2017, Pardo & Mondot, 2018, Sieres *et. al.,* 2021) has been expended. However, these alternatives have not been able to satisfy majority of the fundamental criteria needed for replacement, which, in addition to reduced GWP, are similar or higher volumetric efficiency, similar or improved energy efficiency, and reduced flammability. Additionally, even though a GWP of 750 is the limit set for split AC systems in the EU, automotive ACs already have an upper GWP limit of 150 (Schulz & Kourkoulas, 2014). The authors expect that GWP restrictions for current R410A based systems may fall at or below a GWP limit of 150 soon. Thus, a long-term replacement refrigerant for R410A needs to be found.

R1234ze(E), a pure HFO refrigerant with an ultra-low GWP, has been shown to be a drop-in or light retrofit replacement for R134a systems (see e.g., Fukuda *et. al.* 2014 and Rajendran *et. al.,* 2019). Even though it has a smaller volumetric cooling capacity and latent heat compared to R410A, there are several reasons why it should be considered as a long-term low-GWP replacement for all residential and light commercial applications, including its ultra-low GWP of 7 (Intergovernmental Panel on Climate Change, 2014), good miscibility characteristics with commonly used Polyolester (POE) compressor oils (Jia *et. al.,* 2020) and that it does not form flammable mixtures below 30°C (Mota-Babiloni *et. al.,* 2016), and can thus be considered non-flammable for storage and handling purposes in many climates.

Although substantial research has been completed on vapor compression systems to design next generation HVAC&R equipment for low-GWP fluids (e.g., Li *et. al.*, 2021, Yu *et al.*, 2021), little work exists that looks exclusively at heat exchangers. For light commercial and residential HVAC&R systems, the performance of the two heat exchangers (HXs), *i.e.,* evaporator and condenser, strongly affects the energy efficiency of the unit. Two key performance parameters of fin-and-tube heat exchangers (FTHXs) in air source HPs and ACs are their capacity and pressure drop. Several studies in literature show that both these parameters are heavily dependent on the geometry of the HX, such as circuitry (see e.g., Shen *et. al.*, 2018), and fin density (e.g. Aliabadi *et. al.*, 2014 and Chu *et. al.*, 2020).

This paper supports an improved understanding of the performance effects of R1234ze(E) usage in FTHXs originally designed for R410A. Experiments are performed over a wide range of refrigerant and air side inlet conditions using R410A and R1234ze(E) on a four-circuit FTHX. The experimental data is compared against an advanced segment-by-segment fin-and-tube heat exchanger model called cross-fin (Xfin), which has been extensively validated against R410A (Sarfraz *et. al.,* 2020 and Saleem *et. al.,* 2021). Parametric simulations are then carried out with R1234ze(E) as the working fluid, where fin density and heat exchanger (HX) circuitry are altered independently to evaluate their effect on the HX capacity, superheat (SH), and refrigerant side pressure drop.
.

2. EXPERIMENTAL APPROACH

2.1 Experimental facility and test heat exchanger coil

The experimental facility for this analysis, which is compliant with ASHRAE Standard 33 (2016) for entering air DB temperature uniformity and air face velocity uniformity, and ASHRAE Standard 37 (2016) for air leakage (Saleem *et. al.,* 2021), comprises of:

- A pumped refrigerant loop to control refrigerant conditions at the inlet of test HX coil. It was sized to accommodate test HX coils up to a capacity of 17.5 kW (5 tons) with refrigerant R410A at a saturation suction temperature (SST) of 7.2°C (45°F). The setup is detailed in Saleem *et al.,* (2020).
- A sheet metal coil test duct, insulated by rigid closed cell insulation (R-value of 1.76°C m²/W to ensure heat leakage during testing is reduced to a minimum), and equipped with sampling devices to measure inlet and outlet average air DB and wet-bulb (WB) temperatures, flow straighteners to achieve uniform velocity, and a 5 wide by 3 tall thermocouple grid to measure distribution of entering air temperature at coil face. The construction of a similar test duct to test a different HX coil on this experimental setup has been detailed in Sarfraz *et. al.,* (2020).
- A psychrometric test facility to provide precise control of air dry-bulb (DB) temperature and relative humidity at coil inlet as well as measurement and control of air flowrate (Cremaschi & Lee, 2008).

The tested FTHX coil was designed as an indoor evaporator coil for R410A, having a capacity of 5.5 kW (1.6 ton), at 10°C (50°F) SST, 7.2 K (13 R) superheat, and 0.032 kg/s (250 lbs./hr.) mass flow rate. A circuit schematic of the coil, and key geometrical parameters are shown in Figure 1.

2.2 Test matrix and data reduction

For each experiment with each either of the two fluids, the refrigerant SST, SH, and air inlet velocity ($V_{a,i}$), were chosen as the design factors by using the full factorial design of experiments (Myers & Montgomery, 1995), with refrigerant capacity being the critical outcome. Two modes, dry and wet evaporator operation, were included. The resulting test matrix is shown in Table 1.

The key parameters evaluated from the experiments were the overall refrigerant side capacity, $\dot{Q}_{ref}$, air side capacity, $\dot{Q}_{air}$, bulk SH, $T_{sup,bulk}$, and overall average SH, $T_{sup,avg}$, and are given as,
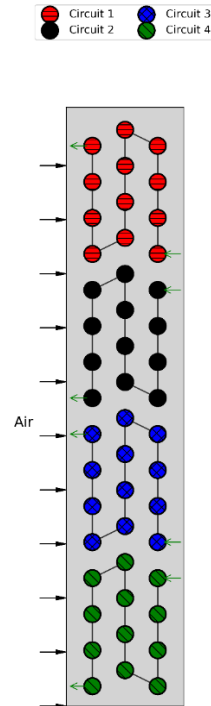
$$\dot{Q}_{ref} = \dot{m}_r \cdot \left(h_{r,out} - h_{r,in} \right) \tag{1}$$

$$T_{sup,bulk} = T_{r,out,bulk} - SST, \text{ and} \tag{2}$$

$$T_{sup,avg} = \frac{\sum_{i=1}^{N} T_{r,out,i}}{N} - SST, \tag{3}$$

$$\dot{Q}_{air} = \dot{m}_{air} \cdot \left(h_{a,bht} - h_{a,aht} \right) \tag{4}$$

Where $\dot{m}_r$ is the refrigerant mass flow rate, $h_{r,in}$ is refrigerant enthalpy at coil inlet, $h_{r,out}$ is refrigerant enthalpy at coil outlet, $T_{r,out,bulk}$ is the refrigerant temperature at coil outlet, N is the total number of circuits in the coil, $T_{r,out,i}$ is the refrigerant temperature at the exit of circuit number i, $\dot{m}_{air}$ is the air mass flow rate, $h_{a,bht}$ and $h_{a,aht}$ are the air enthalpies before and after the coil, respectively.

No. of circuits	4
No. of rows	3
No. of tubes per row	16
No. of tubes per circuit	12
Tube type	Smooth
Tube material	Copper
Tube wall thickness	$0.51 \cdot 10^{-3}$ m
Tube outer diameter	$9.53 \cdot 10^{-3}$ m
Tube longitudinal spacing	$2.19 \cdot 10^{-2}$ m
Tube traverse spacing	$2.54 \cdot 10^{-2}$ m
Tube length	0.593 m
Fin type	Sine wave
Fin thickness	$1.14 \cdot 10^{-4}$ m
Fin spacing	$1.57 \cdot 10^{-3}$ m
Half wavelength of fin wave	$5.51 \cdot 10^{-3}$ m
Wave amplitude	$2.1 \cdot 10^{-3}$ m

Figure 1: Circuit schematic and key geometrical parameters of tested FTHX coil

Table 1: Experimental and simulation test matrix

Refrigerant	Testing mode	Saturated suction temperature (SST)	Air inlet velocity ($V_{a,i}$)	Dry-bulb temperature	Wet-bulb temperature	Superheat (SH)	# of tests
R410A R1234ze(E)	Dry Wet	7.2°C 10.0°C 12.8°C	1 m/s 1.5 m/s 2 m/s	26.7°C	14.4°C[1] 19.4°C[2]	11.1 K	36
Superscripts: 1. For dry evaporator tests 2. For wet evaporator tests							

For refrigerant side capacity, enthalpy is calculated using REFPROP 9 (Lemmon *et. al*., 2018), from measured refrigerant temperatures and pressures at the coil inlet and outlet. To calculate the air side capacity, the enthalpy at inlet and outlet of the coil are required, along with the air mass flow rate. These enthalpies are calculated using CoolProp (Bell *et. al.,* 2014), from the measured air DB and WB temperatures, as well as local total pressure. Details on the type, measurement range, and accuracy of all instrumentation required to measure the required parameters during the experiment are presented in detail in Saleem *et al.,* (2020).

3. SIMULATION RESULTS AND ANALYSIS

3.1 Simulation model validation

HX coil performance was simulated with the Xfin heat exchanger model (Sarfraz *et. al.,* 2019) and then compared against experimental data, collected using processes explained in Section 2.2. Xfin is a discretized HX model, in which the entire HX is broken down into several segments, and each of them is solved for the air and refrigerant side heat transfers by utilizing the ε-NTU method. The Xfin model considers detailed input of the simulated HX's geometry, including circuitry information. Thus, it is an ideal tool to observe how simulated HX performance varies for different geometrical parameters, for the same inlet refrigerant and airside conditions. The Xfin model has been validated against single phase (water) data by Sarfraz *et. al.,* 2019, and for R410A over a wide range of operating conditions and HX geometries in a previous work (Saleem *et. al.,* 2021). This article will extend its validation to R1234ze(E) data. As a point of reference, some key thermodynamic and transport properties of R410A and R1234ze(E) are calculated at 10°C using REFPROP 9 (Lemmon *et. al.,* 2018) and are listed in Table 2.

Table 2: Thermodynamic and transport properties of refrigerants in this analysis, evaluated at 10°C by REFPROP 9

Fluid	P_{sat} (kPa)	ρ_l (kg/m³)	ρ_v (kg/m³)	h_{fg} (kJ/kg)	μ_l (µPas)	μ_v (µPas)
R410A	1088.4	1128.5	41.9	208.6	142.8	12.8
R1234ze(E)	308.4	1210.4	16.5	177.6	238.2	11.6

All information in Figure 1 and Table 1 was provided as inputs to the Xfin model, which then calculated coil capacity, outlet refrigerant SH, and refrigerant side pressure drop. For each of the refrigerants, a literature review identified correlations that were most promising to provide a good match between simulated heat transfer and pressure drop and experimental data. The correlations on refrigerant and air side utilized in the Xfin model simulations are presented in Table 3.

Table 3: Heat transfer and pressure drop correlations used in Xfin model simulations

R410A &	**Heat transfer**	Dittus Boelter equation (Winterton, 1998)
R1234ze(E) **(Single-phase)**	**Pressure drop**	Blasius equation (Blasius, 1913)
R410A	**Heat transfer**	Shah (1982)
(Two-phase)	**Pressure drop**	Lockhart and Martinelli (1949)
R1234ze(E)	**Heat transfer**	Shah (1982)
(Two-phase)	**Pressure drop**	Friedel (1979)
Air	**Heat transfer & pressure drop**	Correlation for wavy fins (Wang *et. al.,* 1997)

Figure 2 (a) and (b) show parity plots comparing experimental and model predicted coil capacities and SH, respectively, for all experiments. The agreement between experimental and simulated capacity is quantified by the MAPE,

$$MAPE = \frac{\left|\dot{Q}_{evap,exp} - \dot{Q}_{evap,sim}\right|}{\dot{Q}_{evap,exp}} \cdot 100\%, \tag{5}$$

where $\dot{Q}_{evap,exp}$, and $\dot{Q}_{evap,sim}$ are the experimental and model predicted refrigerant side capacities, respectively. For comparing the experimental and simulated superheat, the Mean Absolute Error (MAE) is used, given by,

$$MAE = \left|T_{sup,exp} - T_{sup,sim}\right|, \tag{6}$$

where $T_{sup,exp}$, and $T_{sup,sim}$ are the experimental and model predicted refrigerant superheat, respectively.
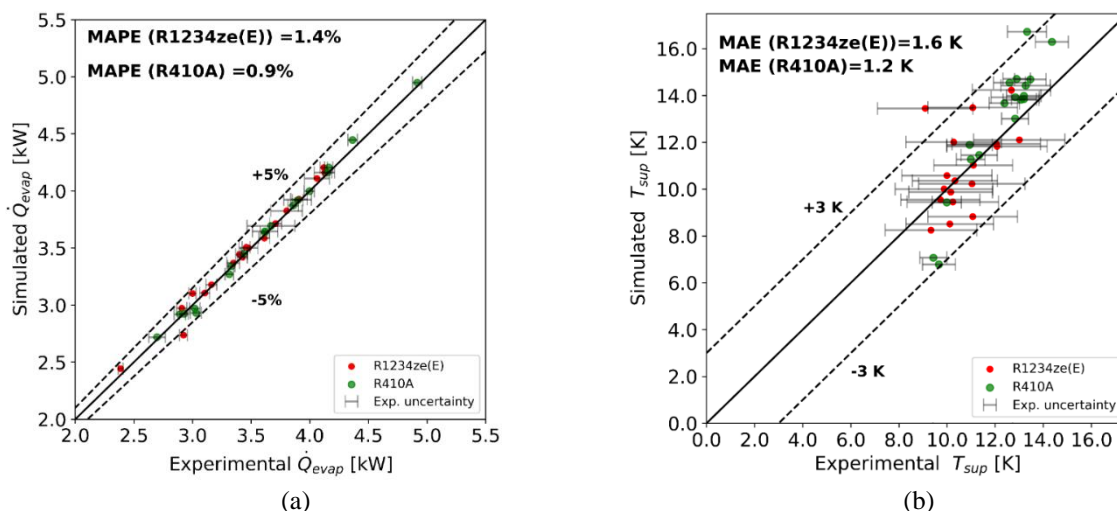
Figure 2: Comparison of experimental and simulated data: (a) refrigerant side capacity, (b) refrigerant SH

The MAPE between experimental and model predicted coil capacity is 1.4% for R1234ze(E), and the MAE between experimental and model predicted superheat is 1.6 K. These validation results provide confidence that any parametric simulation studies done with the Xfin model will have reasonable accuracy with both R410A, as well as R1234ze(E).

3.2 Iterative superheat solver
To compare the performance of R1234ze(E) with R410A, an external root finding algorithm was written, that iterated on the inlet refrigerant mass flow rate until the outlet superheat converged to a set point from the user (within a tolerance of ±1 K). Refrigerant flow rate was the only variable iterated on to achieve the superheat set point, while keeping refrigerant SST and inlet pressure constant.

3.3 Fin density parametric study
The tested HX coil's fin density was 15 FPI (see Figure 1). A upper limit for indoor evaporator FTHX coils' fin density was suggested to be 20 FPI by our industrial collaborators. Thus, a parametric simulation study was performed with fin densities of 15 FPI, 18FPI, and 20 FPI, for the test conditions shown in Table 4.

Figure 3 shows how the fin density effects the HX coil capacity, for three different refrigerant mass flow rates. It also exhibits the relative difference between simulations in dry (relative humidity of 25%) and wet (relative humidity 50%) mode. The term *QP* encapsulates the performance of the simulated heat FTHX,

$$QP = \dot{Q}_{evap} / \Delta P_{ref}. \tag{7}$$

where $\dot{Q}_{evap}$ and ΔP_{ref} are the simulated FTHX capacity and refrigerant side pressure drop, respectively. Table 5 shows the average capacity, superheat, refrigerant side pressure drop, and *QP* for the parametric fin density study.

Table 4: Computational test matrix for fin density parametric analysis

Fluid	Simulation mode	Saturated suction temperature (SST)	Air inlet velocity $(V_{a,i})$	Fin density	# of simulations
R1234ze(E)	Dry Wet	7.22°C	1 m/s 1.5 m/s 2 m/s	15 FPI 18 FPI 20 FPI	18

Figure 3 shows that with increasing fin density, the HX capacity increases, with the increase being more pronounced at higher refrigerant flow rates. Additionally, Table 5 shows that on average, the refrigerant side pressure drop is smaller for greater fin density, resulting in an increase in the value of *QP*. Thus, it can be concluded that increasing fin density for a block circuited HX coil would increase performance and can be hence employed to get optimum or near optimum performance with low-GWP replacements, while keeping all operational parameters identical.
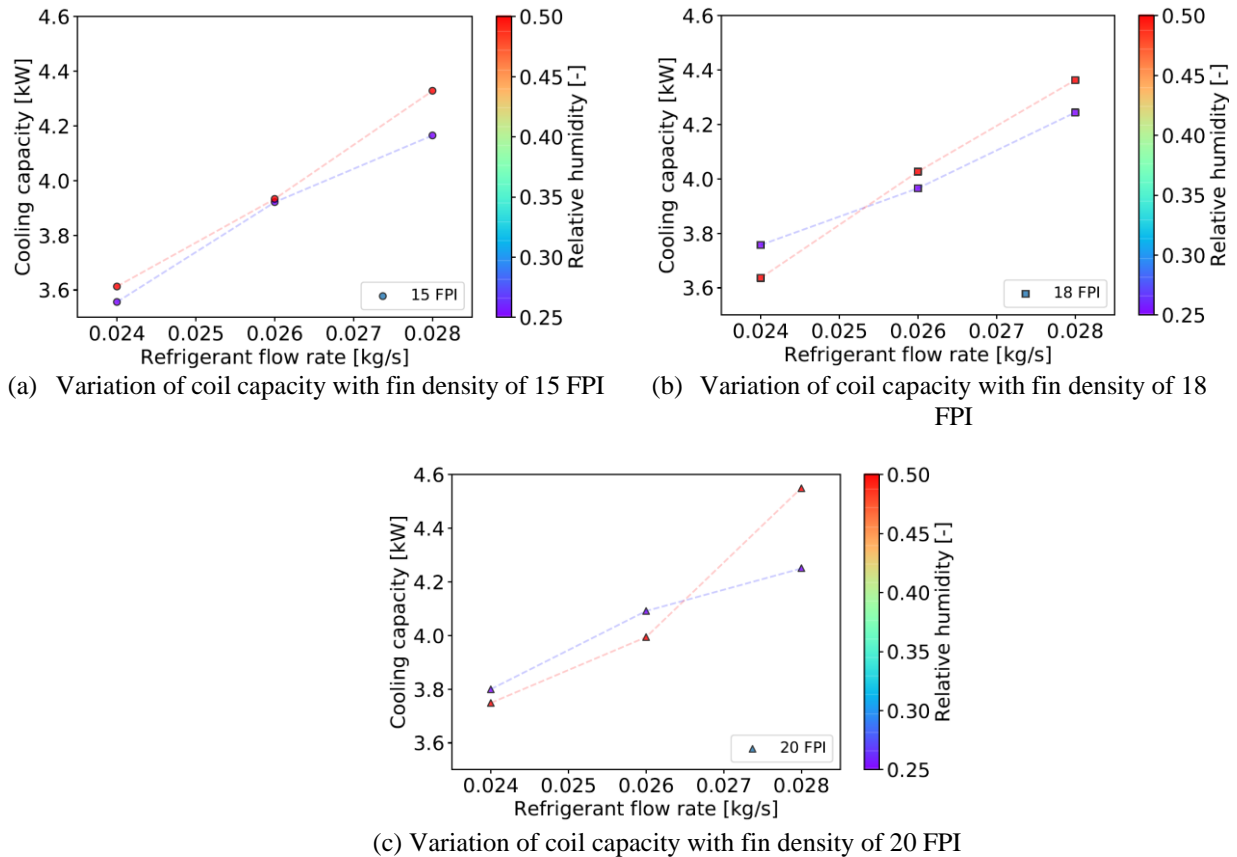
(a) Variation of coil capacity with fin density of 15 FPI

(b) Variation of coil capacity with fin density of 18 FPI

(c) Variation of coil capacity with fin density of 20 FPI

Figure 3: Simulated R1234ze(E) heat exchanger capacity as a function of refrigerant flow rate for fin densities of a) 15 FPI, b) 18 FPI, and c) 20 FPI

Table 5: Average values of simulated HX coil performance as a function of fin density with R1234ze(E)

	15 FPI (baseline)	**18 FPI**	**20 FPI**
Capacity ($\dot{Q}_{evap}$, kW)	3.9	4.0	4.1
Superheat (K)	10.0	9.9	9.5
Refrigerant pressure drop (ΔP_{ref}, kPa)	8.9	8.6	8.5
QP ($\dot{Q}_{evap}/\Delta P_{ref}$, kW/kPa)	0.44	0.47	0.48

3.4 Refrigerant circuitry optimization

To make informed evaluations of refrigerant circuitries that would give the best HX performance, the Xfin model was used in conjunction with the Intelligent System for Heat Exchanger Design (ISHED) module. ISHED comes bundled with EVAP-COND (Domanski *et. al.,* 2016), a tube-by-tube FTHX model, available in the public domain. ISHED was run using the operational parameters listed in Table 6. The goal was to observe how ISHED would optimize the original 4 block circuits of the test HX coil into a minimum of 2 and maximum of 6 circuits, to maximize capacity.
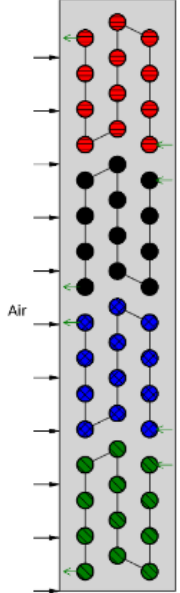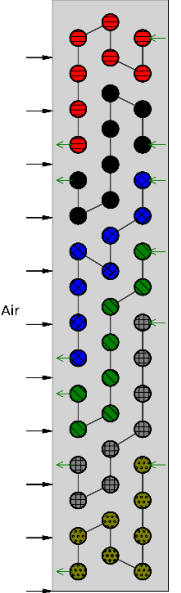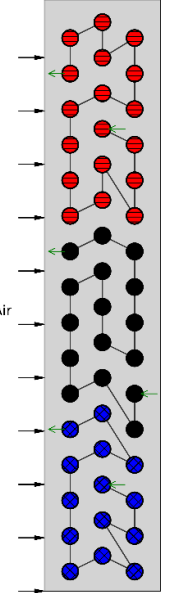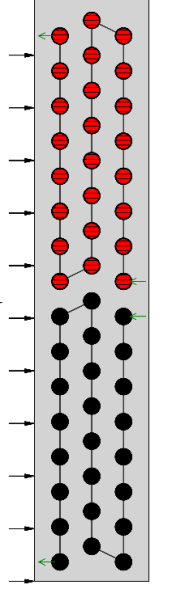
The optimization in ISHED produced several candidate circuitries from which the best two were chosen, and were then evaluated using Xfin, in addition to an un-optimized 2-circuit design with block circuitry. Table 7 shows the results of the Xfin simulations, when run with the operational parameters in Table 6, for each circuitry design.

Table 6: Operational parameters for circuitry optimization in ISHED with R1234ze(E)

Refrigerant				Air		
SST	**Inlet pressure**	**Inlet quality**	**Mass flow rate**	**Inlet DB temperature**	**Inlet relative humidity**	**Volumetric flow rate**
7.2°C	282 kPa	0.305	0.037 kg/s	26.7°C	0.25	0.36 m³/s

The 6-circuit optimized design (ISHED #1) has a 2.5% lower capacity, and 3.6 K lower superheat, in comparison to the original design, but also has significantly lower pressure drop at identical airside heat transfer area. This is caused by a lower per circuit refrigerant flowrate is lower for 6 circuits compared to 4 circuits, and hence the pressure drop is lower. The lower pressure drop can also be accounted to the circuitry pattern, with most tubes having an equal number of first order, i.e., directly adjacent neighboring tubes that carry single phase, and two-phase refrigerant. For this design, the QP was 0.91, which is more than 2.5 times that of the original (baseline) circuitry of the tested HX.

Table 7: Simulated heat exchanger performance in Xfin model with original and optimized refrigerant circuitries; see Table 6 for operational parameters

Circuitry				
	Baseline	ISHED #1	ISHED #2	Manual input
Capacity ($\dot{Q}$, kW)	5.57	5.43	5.52	5.88
Superheat (K)	13.9	10.3	11.7	16.8
Refrigerant pressure drop (ΔP_{ref}, kPa)	15.6	5.9	33.8	116
QP ($\dot{Q}_{evap}/\Delta P_{ref}$, kW/kPa)	0.36	0.91	0.16	0.05

For the 3-circuit design (ISHED #2), it was observed that the capacity and superheat are lower than the original design. This is because the inlet for 2 out of 3 circuits is in the middle row of the HX, a location where the air temperature exiting the tube is not the coldest, and hence the refrigerant capacity in those locations is not utilized to its fullest.

However, it appears that this circuitry design is a compromise to achieve a balance between optimum refrigerant side capacity, and pressure drop. The QP was calculated to be 0.16, 56% lower than the baseline circuitry.

Finally, the un-optimized circuitry design (manual input) led to an increase in capacity of 5.6% more than the original design, but at the expense of pressure drop that was more than 7 times of the original. Despite this high pressure drop causing a drop in refrigerant saturation temperature, this circuitry showed the highest superheat, which is owing to the larger number of passes per circuit, and higher heat transfer area per circuit, when compared to all other circuitry designs. However, the $\dot{Q}/\Delta P$ was only 0.05, making it the poorest design amongst all others. Thus, this illustrates that for refrigerant circuitry modifications, some intuition and artistry may still be required.

4. CONCLUSIONS

This paper presents the influence of fin density and refrigerant circuitry on coil capacity and refrigerant side pressure drop, of a FTHX with R1234ze(E) as the refrigerant. A four-circuit HX coil was tested with R410A and R1234ze(E) in evaporator mode. A total of 36 experiments were caried out with the two fluids, covering a wide range of inlet refrigerant and air side conditions.

Experimental results were compared against model predictions from a discretized fin-and-tube heat exchanger model, called cross-fin (Xfin). For R410A, the MAPE between experimental and simulated coil capacity was 0.9%, and for R1234ze(E), the MAPE between experimental and simulated coil capacity was 1.4%. Simulations were then completed with R410A and R1234ze(E), with a fixed superheat as input to the model, where the fin density of the coil was varied from 15 to 20 FPI. Additionally, the FTHX was simulated with R1234ze(E), for a fixed set of operational parameters with several optimized, and one un-optimized refrigerant circuit design.

Key results obtained in this study are:
- For identical superheat and refrigerant SST, the refrigerant flow rate required for R1234ze(E) was 26% lower than R410A, resulting in 34% lower coil capacities, and 15 times higher refrigerant pressure drop,
- An increase in fin density of 33.3% lead to an increase in capacity of 5.1%, and a reduction in pressure drop of 4.5%,
- For the circuitry which gave a 5.6% increase in capacity compared to the baseline, the refrigerant side pressure drop increased by 7.5 times, whereas the circuitry which gave a 2.5% decrease in capacity (compared to baseline), gave a pressure drop that was 38% lower than the baseline

In the future, the analysis will be extended to include more low-GWP refrigerants, and modification of more HX geometrical parameters, such as tube diameter, tube length, and HX coil face area. This will culminate in a set of design guidelines for FTHX manufacturers, so they can effectively adapt the next generation of their equipment to low-GWP refrigerants for optimum performance.

NOMENCLATURE

AC	Air conditioning	MAPE	Mean Absolute Percent Error
AIM	American Innovation and Manufacturing Act	N	Number of active circuits
COP	Coefficient of Performance	SH	Superheat, K
CFM	Cubic feet per minute	SST	Saturated suction temperature, °C
DB	Dry-bulb	WB	Wet bulb
EPA	Environmental Protection Agency	Xfin	Cross-fin
Evap.	Evaporator	h_{fg}	Latent heat of vaporization, kJ/kg
Exp.	Experimental	$\dot{m}$	Mass flow, kg/s
FPI	Fins per inch	μ	Viscosity, μPas
GWP	Global Warming Potential	ΔP	Pressure drop, kPa
HFC	Hydrofluorocarbon	ρ	Density, kg/m³

HP	Heat Pump	V	Velocity, m/s
ISHED	Intelligent System for Heat Exchanger Design	$\dot{Q}$	Heat transfer/capacity, W
MAE	Mean Absolute Error		

Subscript

a, air	Air	*l*	Liquid
aht	After heat exchanger	*r, ref*	Refrigerant
avg	Average	*sat*	Saturation
bht	Before heat exchanger	*o, out*	Outlet
exp	Experimental	*sim*	Model predicted
i	Circuit number	*sup*	Superheat
in	Inlet	*v*	Vapor

REFERENCES

Aliabadi, M. K., Hormozi, F., & Rad, E. H. (2014). New correlations for wavy plate-fin heat exchangers: Different working fluids. *International Journal of Numerical Methods for Heat and Fluid Flow*, *24*(5), 1086–1108. https://doi.org/10.1108/HFF-09-2012-0195

American Society of Heating, Refrigerant and Air Conditioning Engineers, I. (2016). *ASHRAE Standard 33 - Methods of testing for rating electrically driven unitary air conditioning and heat pump equipment*. Atlanta, USA.

Blasius, H. (1913). Das Ähnlichkeitsgesetz bei Reibungsvorgängen in Flüssigkeiten. Forschungsarbeiten auf dem Gebiete des Ingenieurwesens insbesondere aus den Laboratorien der technischen Hochschulen. Heft 131. Pages 1 to 41. Verein Deutscher Ingenieure. Springer-Verlag Berlin Heidelberg GmbH

Chu, W. X., Sheu, W. J., Hsu, C. C., & Wang, C. C. (2020). Airside performance of sinusoidal wavy fin-and-tube heat exchangers subject to large-diameter tubes with round or oval configuration. *Applied Thermal Engineering*, *164*. https://doi.org/10.1016/j.applthermaleng.2019.114469

Core Writing Team, Pachauri, R. K., & Meyer, L. A. (2014). *Climate Change 2014: Synthesis Report. Contribution of Working Groups I, II and III to the Fifth Assessment Report of the Intergovernmental Panel on Climate Change*. Geneva, Swtizerland.

Cremaschi, L., & Lee, E. (2008). Design and heat transfer analysis of a new psychrometric environmental chamber for heat pump and refrigeration systems testing. *ASHRAE Transactions*, *114*(2), 619–631.

Devecioğlu, A. G. (2017). Seasonal performance assessment of refrigerants with low GWP as substitutes for R410A in heat pump air conditioning devices. *Applied Thermal Engineering*, *125*, 401–411. https://doi.org/10.1016/j.applthermaleng.2017.07.034

Domanski, P., Yashar, D., & Wojtusiak, J. (2016). EVAP-COND, Version 4.0; Simulation Models for Finned-Tube Heat Exchangers with Circuitry Optimization. *NIST/EL*. Retrieved from https://www.nist.gov/publications/evap-cond-version-40-simulation-models-finned-tube-heat-exchangers-circuitry

Friedel, L. (1979). Improved Friction Pressure Drop Correlation for Horizontal and Vertical Two-Phase Pipe Flow. *European Two-Phase Flow Group Meeting, Paper E2*. Ispra.

Fukuda, S., Kondou, C., Takata, N., & Koyama, S. (2014). Low GWP refrigerants R1234ze(E) and R1234ze(Z) for high temperature heat pumps. *International Journal of Refrigeration*, *40*, 161–173. https://doi.org/10.1016/J.IJREFRIG.2013.10.014

Jia, X., Wang, J., Wang, X., Hu, Y., & Sun, Y. (2020). Phase equilibrium of R1234yf and R1234ze(E) with POE lubricant and thermodynamic performance on the evaporator. *Fluid Phase Equilibria*, *514*, 112562. https://doi.org/10.1016/J.FLUID.2020.112562

Lemmon, E. W., Bell, I. H., Huber, M. ., & McLinden, M. O. (2018). *NIST Standard Reference Database 23: Reference Fluid Thermodynamic and Transport Properties-REFPROP, Version 10.0*. https://doi.org/https://dx.doi.org/10.18434/T4JS3C

Li, Z., Shen, B., & Gluesenkamp, K. R. (2021). Multi-objective optimization of low-GWP mixture composition and

heat exchanger circuitry configuration for improved system performance and reduced refrigerant flammability. *International Journal of Refrigeration*, *126*, 133–142. https://doi.org/10.1016/J.IJREFRIG.2021.01.003

Mota-Babiloni, A., Navarro-Esbrí, J., Molés, F., Cervera, Á. B., Peris, B., & Verdú, G. (2016, February 25). A review of refrigerant R1234ze(E) recent investigations. *Applied Thermal Engineering*, Vol. 95, pp. 211–222. https://doi.org/10.1016/j.applthermaleng.2015.09.055

Myers, R. H., & Montgomery, D. C. (1995). *Response Surface Methodology: Process and Product Optimization Using Designed Experiments*. New York: John Wiley and Sons.

Pardo, P., & Mondot, M. (2018). Experimental evaluation of R410A , R407C and R134a alternative refrigerants in residential heat pumps. *International Refrigeration and Air Conditioning Conference*, Paper 2498. Retrieved from https://docs.lib.purdue.edu/cgi/viewcontent.cgi?article=2990&context=iracc

Rajendran, P., Sidney, S., Ramakrishnan, I., & Dhasan, M. L. (2019). Experimental studies on the performance of mobile air conditioning system using environmental friendly HFO-1234yf as a refrigerant: *Https://Doi.Org/10.1177/0954408919881236*, *235*(3), 731–742. https://doi.org/10.1177/0954408919881236

Saleem, S., Bradshaw, C. R., & Bach, C. K. (2021). Validation of a multi-circuit heat exchanger model for evaluating the effect of refrigerant circuitry on cross-fin conduction in evaporator mode. *International Journal of Refrigeration*. https://doi.org/10.1016/J.IJREFRIG.2021.08.015

Saleem, S., Sarfraz, O., Bradshaw, C. R., & Bach, C. K. (2020). Development of novel experimental infrastructure for collection of high-fidelity experimental data for refrigerant to air heat exchangers. *International Journal of Refrigeration*, *114*, 189–200. https://doi.org/10.1016/j.ijrefrig.2020.02.024

Sarfraz, O., Bach, C. K., & Bradshaw, C. (2020). Validation of advanced fin-and-tube heat exchanger models with cross-fin conduction functionality. *International Journal of Refrigeration*, *116*, 70–81.

Sethi, A., & Motta, S. F. Y. (2016). Low GWP Refrigerants for Air-conditioning and Chiller Applications. *International Compressor Engineering, Refrigeration and Air Conditioning, and High Performance Buildings Conferences*, *2*(2013), 1–8.

Shah, M. M. (1982). Chart Correlation for Saturated Boiling Heat Transfer: Equations and Further Study. *ASHRAE Transactions*, Vol. 88, pp. 185–196.

Shen, B., Abdelaziz, O., Shrestha, S., & Elatar, A. (2018). Model-based optimizations of packaged rooftop air conditioners using low global warming potential refrigerants. *International Journal of Refrigeration*, *87*, 106–117. https://doi.org/10.1016/j.ijrefrig.2017.10.028

Sieres, J., Ortega, I., Cerdeira, F., & Álvarez, E. (2021). Drop-in performance of the low-GWP alternative refrigerants R452B and R454B in an R410A liquid-to-water heat pump. *Applied Thermal Engineering*, *182*, 116049. https://doi.org/10.1016/J.APPLTHERMALENG.2020.116049

UNEP. (2016). Amendment to the Montreal Protocol on Substances that Deplete the Ozone Layer, Kigali, 15 October 2016. Retrieved May 22, 2021, from https://ozone.unep.org/treaties/montreal-protocol/amendments/kigali-amendment-2016-amendment-montreal-protocol-agreed

Wang, C. C., Fu, W. L., & Chang, C. T. (1997). Heat transfer and friction characteristics of fin-and-tube heat exchangers. *Experimental Thermal and Fluid Science*, *14*(2), 174–186. https://doi.org/10.1016/S0017-9310(99)00229-X

Winterton, R. H. S. (1998). Where Did the Dittus and Boelter Equation Come From? *International Journal of Heat and Mass Transfer*, (41), 809.

Yu, B., Ouyang, H., SHI, J., LIU, W., & CHEN, J. (2021). Evaluation of low-GWP and mildly flammable mixtures as new alternatives for R410A in air-conditioning and heat pump system. *International Journal of Refrigeration*, *121*, 95–104. https://doi.org/10.1016/j.ijrefrig.2020.09.018

ACKNOWLEDGEMENT